# Symmetry degeneration and room temperature ferroelectricity in ion-irradiated SrTiO 3

F Zhang, Haizhou Xue, J Keum, Alexandre Boulle, Yanwen Zhang, W Weber

# Symmetry degeneration and room temperature ferroelectricity in ion irradiated SrTiO3

F X Zhang[1], Haizhou Xue[2], J K Keum[3], A Boulle[4], Y Zhang[1,2], WJ Weber[1,2]

[1] Materials Science and Technology Division, Oak Ridge National Laboratory, Oak Ridge, TN 37831, United States of America
[2] Department of Materials Science and Engineering, University of Tennessee, Knoxville, TN 37996, United States of America
[3] Center for Nanophase Materials Sciences, Oak Ridge National Laboratory, Oak Ridge, TN 37831, United States of America
[4] Institut de Recherche sur les Céramiques, CNRS UMR 7315, Centre Européen de la Céramique, 12 rue Atlantis, 87068 Limoges Cedex, France

**Abstract**

Polar phonon modes associated with room temperature ferroelectricity are observed in $SrTiO_3$ single crystals irradiated with Ti ions. Quantitative strain analysis reveals that irradiation-induced out-of-plane strain drives the centrosymmetric cubic $SrTiO_3$ to a tetragonal-like structure in the maximum damaged region. Energy transfer from ions to electrons during ion irradiation yields defects in $SrTiO_3$ that also plays an important role for the room temperature ferroelectricity. Different from thin film techniques, the ferroelectricity in the ion irradiated $SrTiO_3$ can occur for much larger thicknesses, depending on the energy and type of ion.

## 1. Introduction

Bulk $SrTiO_3$ has a centrosymmetric cubic structure at room temperature, and there is a cubic to tetragonal structural transition at 105 K [1]. The dielectric constant of $SrTiO_3$ deviates from the classical Curie–Weiss law at low temperature, and it increases rapidly (up to $1.8 \times 10^4$ at 1.4 K) as the temperature is reduced [2]. The low temperature electric behavior of $SrTiO_3$ approaches a ferroelectric phase transition; however, bulk $SrTiO_3$ is still paraelectric to the lowest temperature as a result of quantum fluctuations [3]. The 'quantum paraelectrics' or 'incipient ferroelectronics' of $SrTiO_3$ and other perovskite oxides have been a topic of considerable interest during the past few decades [3–5].

The ferroelectric transition of $SrTiO_3$ at low temperature can be induced by strains from lattice mismatch [5, 6], chemical [7, 8] or isotopic [9] substitution, electric field [10, 11], pressure [14] and controlled grain size [12]. Due to important applications in electronic devices, the coupling between strain and ferroelectricity in $SrTiO_3$ films has been intensively studied, and the relevant work is well illustrated in a recent review article [13]. By controlling the in-plane lattice strain, the critical temperature $T_c$ of ferroelectric transition in thin film $SrTiO_3$ or superlattice can be profoundly enhanced [6, 14–18], even to room temperature [5]. However, the biaxial strains in thin films depend on the choice of substrate and film thickness, which turns out to be challenging for the synthesis of uniformly strained films because of the undesirable relaxation that occur when the thickness of a sample exceeds the

critical value. Room temperature ferroelectricity has also been reported for nonstoichiometric $SrTiO_3$ films with controlled Sr or O deficiencies [19, 22], though the mechanism is still under debate [15, 20, 21].

One fundamental property of ferroelectrics that changes quantitatively during phase transition is the dynamics of lattice vibration. The lattice dynamics of bulk $SrTiO_3$ has been studied theoretically and experimentally with neutron scattering techniques decades ago [22]. As a powerful tool to study the lattice properties, Raman scattering has been successfully used to detect the symmetry degeneration and phase transition in $SrTiO_3$. Since all the zone-center optical phonons of the ideal cubic $SrTiO_3$ are of odd parity, no first-order Raman scattering is expected to occur at ambient conditions. Instead, broad second-order peaks are observed in the wavelength ranges of 200–500 $cm^{-1}$ and 550–750 $cm^{-1}$. Using an ultraviolet Raman spectroscopy technique, nanoscale ferroelectricity was successfully probed in ultrathin films of $BaTiO_3/SrTiO_3$ superlattice [23]. In the present work, we studied the response of ⟨001⟩-oriented $SrTiO_3$ single crystals to ion irradiation with Raman scattering and x-ray diffraction techniques. The appearance of forbidden optical phonon modes in the damaged regions suggests room temperature ferroelectricity in the ion-irradiated $SrTiO_3$. The strain depth profile in ion irradiated $SrTiO_3$ is quantitatively analyzed by single crystal x-ray diffraction measurements, and the results indicate a large tetragonal distortion with a significant out-of-plane lattice strain (1.1–1.3%) and negligible in-plane strain. The tetragonal distortion promotes the ferroelectric transition of ion irradiated $SrTiO_3$. The defects in the lattice induced by the energy transfer from Ti ions to the electronic structure also plays an important role for the ferroelectric transition in $SrTiO_3$ crystals.

## 2. Experimental procedure

The ⟨001⟩-oriented single crystals of $SrTiO_3$, with size of 12 × 15 $mm^2$, were irradiated at room temperature with 12 MeV or 20 MeV Ti ions to fluences from $1 \times 10^{12}$ to $1 \times 10^{14}$ $cm^{-2}$, with multiple irradiated areas of 3 × 3 $mm^2$ per sample. The ion irradiations were performed at several degrees off the surface normal to avoid channeling effects using the capabilities of the Ion Beam Materials Laboratory at the University of Tennessee [24]. The Raman spectra from the $SrTiO_3$ were collected in a reflection configuration using a high-resolution Raman spectrometer (LabRaman HR Evolution) at room temperature with a 532 nm green laser as the activation light. Irradiation-induced strain along the direction normal to the ⟨001⟩-oriented surface was measured with a high-resolution thin film x-ray diffractometer (PANalytical X'pert Pro) in 2θ–θ scan mode with Cu Kα1 x-ray radiation (λ = 1.5406 Å). The strain profiles for samples irradiated with 12 MeV Ti ions were derived from simulation of the XRD patterns with the program RaDMaX [25]. Reciprocal space maps were also recorded for the symmetric (002) and asymmetric (103) lattice planes of the samples irradiated with both 12 MeV and 20 MeV Ti ions, and the latter being used to determine the in-plane lattice strain.

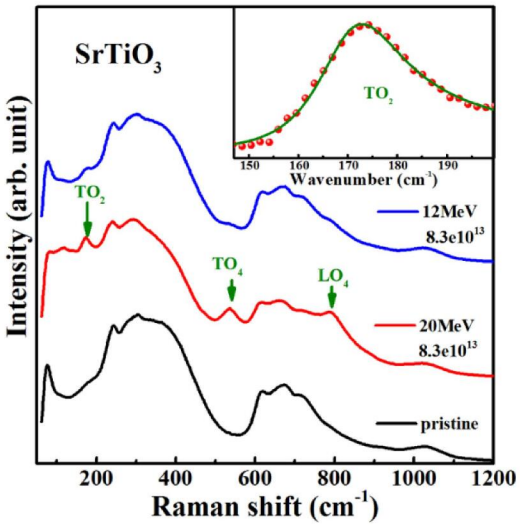


**Figure 1.** (a) The observed Raman spectrum of pristine $SrTiO_3$ and damaged with Ti ions of 12 MeV and 20 MeV in fluence of $8.3 \times 10^{13}$ ions $cm^{-2}$. (b) The fitting of the Fano asymmetry Raman modes $TO_2$ and $TO_4$ for the 20 MeV Ti ions irradiated sample. The Fano fitting parameters are $A = 39.15$, $q = 4.11$, $\omega_0 = 170.2$ $cm^{-1}$, and $\Gamma = 21.98$ $cm^{-1}$.

## 3. Results and discussion

All the irradiated spots were characterized by Raman scattering measurements. There is only second-order Raman scattering signal in pristine $SrTiO_3$ because of the centrosymmetric structure. We observed additional Raman active modes in the irradiated samples, especially for the 20 MeV Ti ion irradiated spots. Figure 1 shows the Raman spectrum of $SrTiO_3$ irradiated with 12 MeV and 20 MeV Ti ions to a fluence of $8.3 \times 10^{13}$ $cm^{-2}$, together with the spectrum from the pristine sample. The additional modes appearing in the sample irradiated with 20 MeV Ti ions are the polar transverse optic modes $TO_2$, $TO_4$ and polar longitudinal $LO_4$ modes, which are centered at ~170, 550 and 800 $cm^{-1}$, respectively. The appearance of these polar phonon modes in the irradiated samples is similar to the modes observed in ferroelectric films before [23, 26, 27], which is an indication of ferroelectricity. The corresponding phonon modes in the 12 MeV irradiated $SrTiO_3$ are weaker. In the 20 MeV Ti ion irradiated sample, there is a weak peak centered at ~140 $cm^{-1}$, which is the $e_g$ mode of tetragonal $SrTiO_3$ [28]. Similar to the Raman spectrum of strained $SrTiO_3$ thin films, the appearance of the first-order Raman modes is due to breaking of the symmetry after ion irradiation. The ferroelectricity is caused by the polarization displacement of cations and anions in the damaged region. As observed in thin films [18] and nano-structured $SrTiO_3$ [12], a pronounced Fano asymmetric peak shape is seen for the $TO_2$ mode, which suggests coherent interference between the discrete phonon and a broad peak [29]. The Fano $TO_2$ mode in ion irradiated $SrTiO_3$ single crystal can also be fitted by the formula

$$I(\omega) = A\frac{[q + E(\omega)]^2}{1 + E(\omega)^2}$$

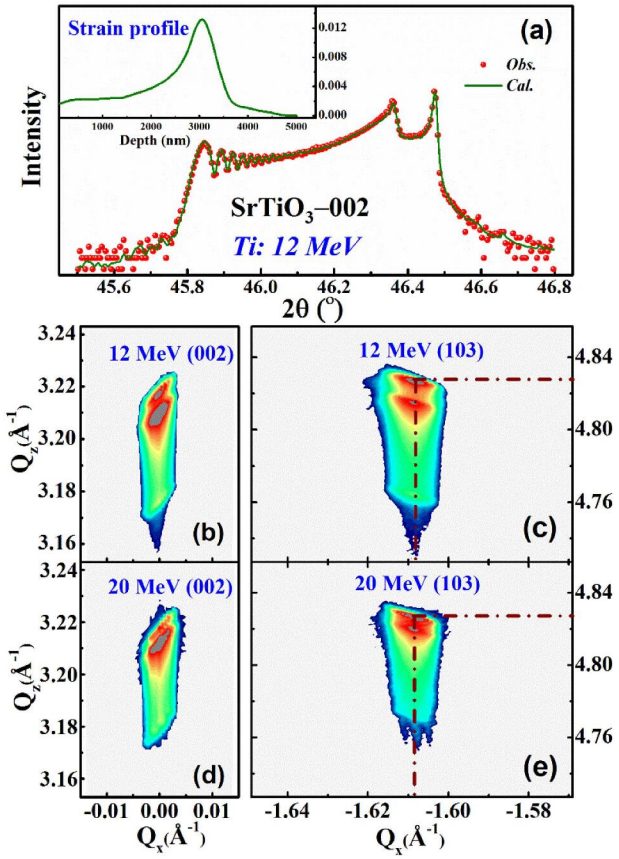


**Figure 2.** (a) The observed and calculated XRD profiles of the 12 MeV Ti ion irradiated $SrTiO_3$ around the Bragg peak (002). The maximum strain is ~1.32%, and the corresponding depth dependent strain profiles are shown as inserts; (b) and (c) the reciprocal space maps of 12 MeV Ti ion irradiated sample around the (002) and (103) Bragg peaks; (d) and (e) the reciprocal space maps of 20 MeV Ti ion irradiated $SrTiO_3$ near the lattice point of (002) and (103).

after subtracting a constant base line, where $E(\omega) = 2(\omega - \omega_0)/\Gamma$, and $\omega_0$ is the phonon frequency, $A$ is the amplitude, $\Gamma$ is the full width at half maximum, and $q$ is the asymmetry parameter. The fitting of $TO_2$ mode is shown as the insert of figure 1, and the phonon frequency is 170.2 $cm^{-1}$.

In order to measure the radiation-induced lattice strain, the samples were characterized using single crystal x-ray diffraction in a symmetric scan mode. Figure 2(a) shows the (002) Bragg peak of $SrTiO_3$ after 12 MeV Ti ion irradiation to a fluence of $8.3 \times 10^{13}$ ions $cm^{-2}$. The x-ray beam penetrates the whole damaged layer, and the sharp peak in the high angle side is the Bragg peak from the undamaged part. The broad signal with lower $2\theta$ angle comes from the damaged layers. The fringe features indicate the presence of a damage-induced dilation gradient in the direction normal to the sample surface [30]. The simulation of the diffraction pattern allows us to derive the depth-strain profile. As shown by the insert in figure 2(a), the derived strain profile yields a good fit to the measured XRD pattern. The maximum strain occurs at depth of ~3000 nm, which is in good agreement with the predicted damage profile based on SRIM calculations [31].The lattice expansion along $\langle 001 \rangle$ from ion irradiation has a maximum out-of-plan strain of 1.32%. Unlike thin films, it is usually observed that there is no in-plane strain for ion-irradiated crystals [32]. In order to determine the in-plane lattice strain, reciprocal space maps (RSMs) were measured for both the symmetric (002) and asymmetric (103) Bragg peak (figures 2(b) and (c)). The RSM of the asymmetric (103) peak shows only damage perpendicular to the sample surface. The scattering from both the damaged and undamaged region exhibit an identical value of $Q_x$ coordinate which demonstrates that the lattice expansion parallel to the surface is negligible. The lattice strain can also be estimated from the RSMs. The maximum lattice strain for the sample irradiated with 12 MeV Ti ions is 1.31% and 1.30%, as estimated from the (002) and (103) RSMs, respectively. The maximum lattice strain estimated from RSMs is in good agreement with the one-dimensional XRD measurement. Similar measurements were performed for the sample irradiated with 20 MeV Ti ions. The XRD profile around the (002) Bragg peak shows the damage peak without well-resolved fringes which forbids a reliable simulation. The RSMs around (002) and (103) Bragg peaks are shown in figures 2(d) and (e), respectively. With a similar analysis, the maximum lattice strain in the sample irradiated with 20 MeV Ti ions is estimated to be 1.13% from both (002) and (103) RSMs. As shown in the depth dependent strain profile (figure 2(a)), ion irradiation induced damage is not homogeneous along the path of the ions and, near the sample surface, the out-of-plane lattice strain is relatively weak (<0.03%). It is thus important to check the structure in the whole damaged region. The maximum strain induced by 20 MeV Ti ion irradiation is slightly less than that for 12 MeV Ti ions, which indicates that the tetragonal distortion for 12 MeV Ti is larger than for 20 MeV Ti, at least in the maximum damaged region. However, the Raman spectrum (figure 1) clearly shows more ferroelectricity in the 20 MeV ion irradiated sample. This inconsistency suggested that symmetry breaking is not the only reason for the ferroelectric transition in ion irradiated $SrTiO_3$ crystals.

Figure 3(a) shows the depth dependent Raman spectrum from the $SrTiO_3$ sample irradiated with 20 MeV Ti ions over the whole damaged depth (<6 μm) with incremental depth measurement steps of 0.3 μm. The feature of ferroelectricity is clearly observed from the top to the maximum damaged depth (~3–4 μm). Beside the appearance of $TO_2$, $TO_4$ and $LO_4$ modes, the second-order Raman modes shift the center positions at different depths. As shown by the dashed guidelines in figure 3(a), the modes have red shifted gradually from surface to the maximum damaged depth of ~3.9 μm, then quickly switched back to higher wavenumber values, as in the pristine sample. This is an indication of the inhomogeneous lattice expansion with depth, and the maximum damaged region has the minimum wavenumber because of the maximum lattice expansion. The positions of the new phonon modes are not sensitive to depth or damage levels. After the Fano fit, however, the frequency of the $TO_2$ mode has undergone an observable shift (<2 $cm^{-1}$) due to the change of peak shape. In the maximum damaged region (2.4–3.3 μm), the peak position is nearly the same as the Fano fit (figure 3(b)). The symmetric $TO_4$ mode fitted with a Gaussian function shows no significant shift (<1 $cm^{-1}$) from surface to the maximum damaged

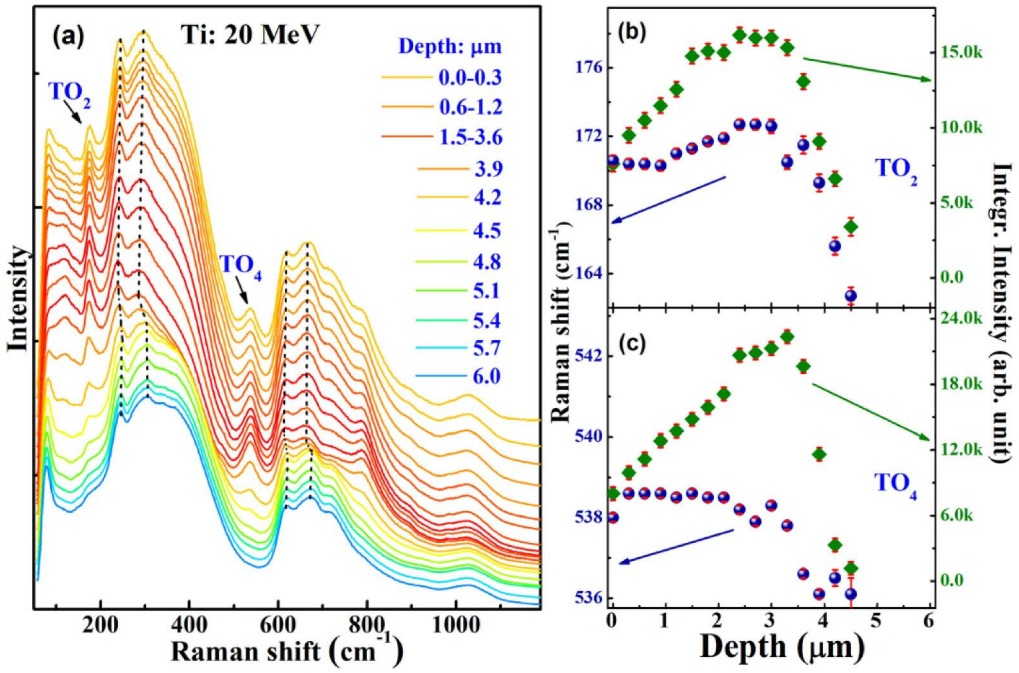


**Figure 3.** (a) The depth dependent Raman spectrum of $SrTiO_3$ irradiated with 20 MeV Ti ions. (b) and (c) The wavenumber and peak intensity of $TO_2$ mode with Fano asymmetry f tting and $TO_4$ mode with Gaussian f tting respectively.

region (f gure 3(c)). The intensity of both $TO_2$ and $TO_4$ modes increase with depth from the surface to the maximum damaged depth and then drops dramatically and eventually disappear. The cross-sectional Raman spectrum clearly indicates that the ferroelectricity starts from the very top surface to the maximum damaged region. The maximum damaged region has a tetragonal character, which can be seen from the weak tetragonal modes centered at 140 $cm^{-1}$ and 478 $cm^{-1}$, respectively. After the maximum damage, the intensity of all the new modes dropped rapidly, this is consistent with the damage prediction by SRIM, as discussed later. The depth dependent Raman spectrum also suggests that symmetry degeneration in the maximum damaged region is not the only reason of the ferroelectric transition in $SrTiO_3$ crystal.

Raman spectrum (f gure 1) clearly indicates ferroelectric transition in $SrTiO_3$ is dependent on the ion energies, and the ferroelectric feature of 20 MeV Ti ion irradiated sample is more obvious than that in 12 MeV Ti ion irradiated samples. Figure 4 illustrates the energy deposition and damage levels (displacement per atom) for $SrTiO_3$ irradiated with 20 MeV and 12 MeV Ti ions at room temperature based on full-cascade SRIM calculations [33]. Except for the different ion penetration depths, the damage levels for 20 MeV and 12 Mev Ti ion irradiation of $SrTiO_3$ are similar (~0.05 dpa). The elastic energy loss to atomic nuclei in $SrTiO_3$ is very small (<0.1 keV $nm^{-1}$) in the f rst 1 μm region and <0.7 keV $nm^{-1}$ in the maximum damage region. The much larger energy loss to the electrons is an inelastic process, and the effect on the lattice damage is not well understood [34]. Previous studies have shown that it has a complicated effect on the lattice, it can generate defects and, in the meanwhile, the strong electron–phonon coupling can also cause damage recovery, like

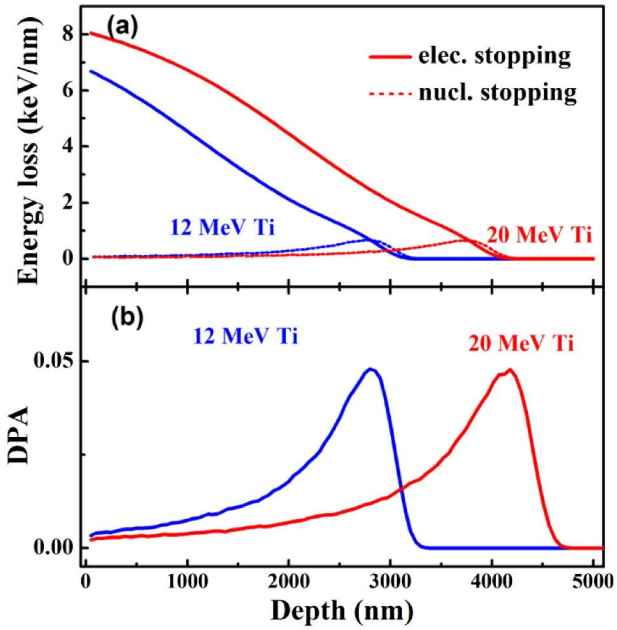


**Figure 4.** The calculated energy loss (a) and damage (b) in $SrTiO_3$ crystal irradiated with 12 MeV and 20 MeV Ti ions.

for MeV ions irradiated SiC [35]. A synergistic effect of electronic energy loss with pre-existing defects in $SrTiO_3$ has been conf rmed experimentally and theoretically [34, 36], and amorphous tracks and additional defects are generated in the predamaged crystal samples. High electron energy loss induces a localized thermal spike that can cause local melting of the sample along He ion path to form amorphous tracks via rapid quenching. The threshold in electron energy loss for forming

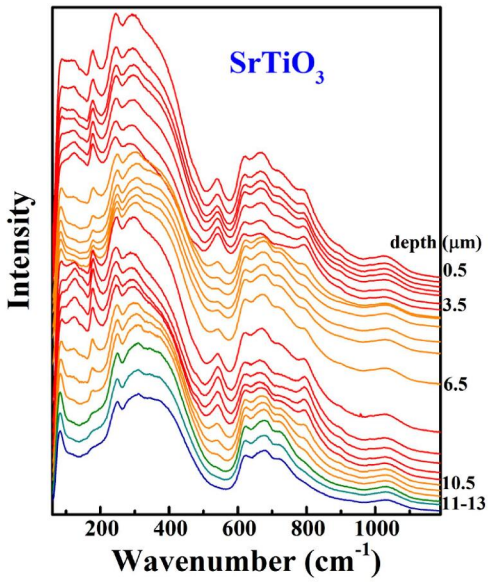


**Figure 5.** Cross section Raman spectrum of $SrTiO_3$ irradiated with 20 MeV Ti ions in fluence of $1 \times 10^{14}$ $cm^{-2}$, and then measured with RBS, which the sample was bombard with 3.5 MeV He ions. The ferroelectricity layer has a thickness more than 10 μm, and the step of depth is 0.5 μm before 10.5 μm and 1 μm after 11 μm.

tracks in pristine $SrTiO_3$ is ~12.7 keV $nm^{-1}$ [37]; however, in the case of slightly pre-damaged $SrTiO_3$, the threshold for amorphous track formation decreases significantly to about 6.5 keV $nm^{-1}$ [36, 38]. While the electron energy loss of 12 MeV and 20 MeV Ti ions is less than the threshold for amorphous track formation in pristine $SrTiO_3$, their electronic energy loss is above the threshold for amorphous track formation in the presence of pre-existing defects. Thus, a delayed formation of amorphous tracks may occur once a sufficient concentration of defects accumulate due to nuclear collision processes, as has been observed in $LiTaO_3$ [39]. Since the electronic energy loss for 20 MeV Ti ions (figure 4(b)) is obviously higher than that for 12 MeV Ti ions, more damage production in the form of amorphous tracks and defects is expected for 20 MeV Ti ions. The damage due to the electronic energy loss may be directly related to the ferroelectric transition in $SrTiO_3$ crystals.

Room temperature ferroelectricity has been reported in non-stoichiometric $SrTiO_3$ thin films by controlling the oxygen deficiencies [19, 34]. Kim [20] has proposed the formation of a defect dipole by Sr–O–O clusters, which may be the possible origin of room temperature ferroelectricity in non-stoichiometric $SrTiO_3$ films. In addition to the tendency of a tetragonal structural transition, the room temperature ferroelectricity in $SrTiO_3$ due to Ti ion irradiation may have a similar origin, because oxygen vacancies can be easily generated by MeV ion irradiation. Previous photoluminescence and x-ray absorption measurements [41, 42] have suggested that ion irradiation of $SrTiO_3$ readily yields oxygen vacancy disorder and near-surface irradiation of $SrTiO_3$ with Ar ions also creates an oxygen deficiency [43].

Compared to thin film techniques, ion irradiation can make room temperature ferroelectricity in $SrTiO_3$ over much larger thicknesses. Figure 5 shows the depth dependent Raman spectrum from $SrTiO_3$ irradiated with 20 MeV Ti ions to a dose of $1 \times 10^{14}$ $cm^{-2}$, and then subsequently irradiated with 3.5 MeV He ions for Rutherford backscattering spectroscopy measurements. The ferroelectricity is observed to a depth of ~10 μm. Two maxima in the damaged regions due to 20 MeV Ti ions and 3.5 MeV He ions irradiation are clearly seen from the Raman spectra. By irradiating with ions of high energies, such as swift heavy ions, it is expected that much thicker or even bulk $SrTiO_3$ can be transformed to ferroelectric state at room temperature.

## 4. Conclusions

Room temperature ferroelectricity was detected by Raman scattering in $SrTiO_3$ irradiated with Ti ions. X-ray diffraction measurements suggest that the transition is due to symmetry breaking, which caused by the large out-of-plane strains. $SrTiO_3$ irradiated with 20 MeV Ti ions shows more profound transition features than the sample irradiated with 12 MeV Ti ions. Ion irradiation induced damage, especially the formation of oxygen vacancies, may play an important role for the ferroelectric transition in $SrTiO_3$.

## Acknowledgments

FZ would like to acknowledge the help from Dr Aurelien Debelle for the x-ray measurements and strain analysis. This work was supported by the U.S. Department of Energy, Office of Science, Basic Energy of Sciences, Materials Sciences and Engineering Division under Contract DE-AC05-00OR22725. HX was supported by the University of Tennessee Governor's Chair program for RBS/C. The lab x-ray experiment was conducted at the Center for Nanophase Materials Sciences, which is a DOE Office of Science User Facility.

## References

[1] Rimai L and Demars G A 1962 Electron paramagnetic resonance of trivalent gadolinium ions in strontium and barium titanates *Phys. Rev.* **127** 702–10

[2] Weaver H E 1959 Dielectric properties of single crystals of $SrTiO_3$ at low temperatures *J. Phys. Chem. Solids* **11** 274–77

[3] Müller K A and Burkard H 1979 $SrTiO_3$: an intrinsic quantum paraelectric below 4 K *Phys. Rev.* B **19** 3593–602

[4] Fujishita H, Kitazawa S, Saito M, Ishisaka R, Okamoto H and Yamaguchi T 2016 Quantum paraelectric states in $SrTiO_3$ and $KTaO_3$: Barrett model, Vendik model, and quantum criticality *J. Phys. Soc. Jpn.* **85** 074703

[5] Haeni J H *et al* 2004 Room-temperature ferroelectricity in strained $SrTiO_3$ *Nature* **430** 758–61

[6] Uwe H and Sakudo T 1976 Stress-induced ferroelectricity and soft phonon mode in $SrTiO_3$ *Phys. Rev.* B **13** 271

[7] Ouillon R, Pinan-Lucarre J-P, Ranson P, Pruzan P, Mishra S K, Ranjan R and Pandey D 2002 A Raman scattering study of the phase transitions in $SrTiO_3$ and in the mixed system $(Sr_{1-x}Ca_x)TiO_3$ at ambient pressure from $T = 300$ K down to 8 K *J. Phys.: Condens. Matter* **14** 2079–92

[8] Bianchi U, Kleemann W and Bednorz J G 1994 Raman scattering investigation of $Y_{1-x}Ca_xTiO_3$ *J. Phys.: Condens. Matter* **6** 1229–38

[9] Itoh M, Wang R, Inaguma Y, Yamaguchi T, Shan Y J and Nakamura T 1999 Ferroelectricity induced by oxygen isotope exchange in strontium titanate perovskite *Phys. Rev. Lett.* **82** 3540–3

[10] Fleury P A, Scott J F and Worlock J M 1968 Soft phonon modes and the 110 K phase transition in $SrTiO_3$ *Phys. Rev. Lett.* **21** 16–9

[11] Worlock J M and Fleury P A 1967 Electric f eld dependence of optical-phonon frequencies *Phys. Rev. Lett.* **19** 1176–9

[12] Banerjee S, Kim D I, Robinson R D, Herman I P, Mao Y and Wong S S 2006 Observation of Fano asymmetry in Raman spectra of $SrTiO_3$ and $Ca_xSr_{1-x}TiO_3$ perovskite nanocubes *Appl. Phys. Lett.* **89** 223130

[13] Pai Y, Tylan-Tyler A, Irvin P and Levy J 2018 Physics of $SrTiO_3$–based heterostructures and nanostructures: a review *Rep. Prog. Phys.* **81** 036503

[14] Li Y L *et al* 2006 Phase transitions and domain structures in strained pseudocubic (100) $SrTiO_3$ thin f lms *Phys. Rev.* B **73** 183112

[15] Jang H W *et al* 2010 Ferroelectricity in strain-free $SrTiO_3$ thin f lms *Phys. Rev. Lett.* **104** 197601

[16] Akimov I A, Sirenko A A, Clark A M, Hao J H and Xi X X 2000 Electric-f eld-induced soft-mode hardening in $SrTiO_3$ Films *Phys. Rev. Lett.* **84** 4625–8

[17] Sirenko A A, Bernhard C, Golnik A, Clark A M, Hao J, Si W and Xi X X 2000 Soft-mode hardening in $SrTiO_3$ thin f lms *Nature* **404** 373–6

[18] Sirenko A A, Akimov I A, Fox J R, Clark A M, Li H C, Si W and Xi X X 1999 Observation of the f rst-order Raman scattering in $SrTiO_3$ thin f lms *Phys. Rev. Lett.* **82** 4500–3

[19] Yang F, Zhang Q, Yang Z, Gu J, Liang Y, Li W, Wang W, Jin K, Gu L and Guo J 2015 Room-temperature ferroelectricity of $SrTiO_3$ f lms modulated by cation concentration *Appl. Phys. Lett.* **107** 082904

[20] Kim Y S, Kim J, Moon S J, Choi W S, Chang Y J, Yoon J G, Yu J, Chung J S and Noh T W 2009 Localized electronic states induced by defects and possible origin of ferroelectricity in strontium titanate thin f lms *Appl. Phys. Lett.* **94** 202906

[21] Choi M, Oba F and Tanaka I 2009 Role of Ti antisitelike defects in $SrTiO_3$ *Phys. Rev. Lett.* **103** 185502

[22] Cowley R A 1964 Lattice dynamics and phase transitions of strontium titanate *Phys. Rev.* **134** A981–7

[23] Tenne D A *et al* 2016 Probing nanoscale ferroelectricity by ultraviolet Raman spectroscopy *Science* **313** 1614–6

[24] Zhang Y, Crespillo M, Xue H, Jin K, Chen C H, Fontana C L, Graham J T and Weber W J 2014 New ion beam materials laboratory for materials modif cation and irradiation effects research *Nucl. Instrum. Methods Phys. Res.* B **338** 19–30

[25] Souilah M, Boulle A and Debelle A 2016 Computer programs RaDMaX: a graphical program for the determination of strain and damage prof les in irradiated crystals *J. Appl. Crystallogr.* **49** 311–6

[26] Rychetský I *et al* 2001 Dielectric, infrared, and Raman response of undoped $SrTiO_3$ ceramics: evidence of polar grain boundaries *Phys. Rev.* B **64** 184111

[27] Ostapchuk T *et al* 2002 Origin of soft-mode stiffening and reduced dielectric response in $SrTiO_3$ thin f lms *Phys. Rev.* B **66** 235406

[28] Perry C H, Fertel J H and McNelly T F 1967 Temperature dependence of the Raman spectrum of $SrTiO_3$ and $KTaO_3$ *J. Chem. Phys.* **47** 1619–25

[29] Fano U 1961 Effects of integration on intensities and phase shifts *Phys. Rev.* **124** 1866–78

[30] Thomé L, Velisa G, Miro S, Debelle A, Garrido F, Sattonnay G, Mylonas S, Trocellier P and Serruys Y 2015 Recovery effects due to the interaction between nuclear and electronic energy losses in SiC irradiated with a dual-ion beam *J. Appl. Phys.* **117** 105901

[31] Ziegler J F 2004 SRIM-2003 *Nucl. Instrum. Methods Phys. Res.* B **219–220** 1027–36

[32] Debelle A and Declémy A 2010 XRD investigation of the strain/stress state of ion-irradiated crystals *Nucl. Instrum. Methods Phys. Res.* B **268** 1460–5

[33] Weber W J and Zhang Y 2019 Predicting damage production in monoatomic and multi-elemental targets using stopping and range of ions in matter code: challenges and recommendations *Curr. Opin. Solid State Mater. Sci.* **23** 100757

[34] Weber W J, Zarkadoula E, Pakarinen O H, Sachan R, Chisholm M F, Liu P, Xue H, Jin K and Zhang Y 2015 Synergy of elastic and inelastic energy loss on ion track formation in $SrTiO_3$ *Sci. Rep.* **5** 7726

[35] Zhang Y, Sachan R, Pakarinen O H, Chisholm M F, Liu P, Xue H and Weber W J 2015 Ionization-induced annealing of pre-existing defects in silicon carbide *Nat. Commun.* **6** 8049

[36] Xue H, Zarkadoula E, Liu P, Jin K, Zhang Y and Weber W J 2017 Amorphization due to electronic energy deposition in defective strontium titanate *Acta Mater.* **127** 400–6

[37] Karlusic M, Akcoltekin S, Osmani O, Monnet I, Lebius H, Jaksic M and Schleberger M 2010 Energy threshold for the creation of nanodots on $SrTiO_3$ by swift heavy ions *New J. Phys.* **12** 043009

[38] Xue H, Zarkadoula E, Sachan R, Zhang Y, Trautmann C and Weber W J 2018 Synergistically-enhanced ion track formation in pre-damaged strontium titanate by energetic heavy ions *Acta Mater.* **150** 351–9

[39] Sellami N, Crespillo M L, Zhang Y and Weber W J 2018 Two-stage synergy of electronic energy loss with defects in $LiTaO_3$ under ion irradiation *Mater. Res. Lett.* **6** 339–44

[40] Lee S A *et al* 2016 Phase transitions via selective elemental vacancy engineering in complex oxide thin f lms *Sci. Rep.* **6** 23649

[41] Crespillo M L, Graham J T, Agulló-López F, Zhang Y and Weber W J 2017 Correlation between $Cr^{3+}$ luminescence and oxygen vacancy disorder in strontium titanate under MeV ion irradiation *J. Phys. Chem.* C **121** 19758–66

[42] Sabathier C, Chaumont J, Rouzière S and Traverse A 2005 Characterisation of Ti and Sr atomic environments in $SrTiO_3$ before and after ion beam irradiation by x-ray absorption spectroscopy *Nucl. Instrum. Methods Phys. Res.* B **234** 509–19

[43] Kan D, Terashima T, Kanda R, Masuno A, Tanaka K, Chu S, Kan H, Ishizumi A, Kanemitsu Y, Shimakawa Y and Takano M 2005 Blue-light emission at room temperature from $Ar^+$-irradiated $SrTiO_3$ *Nat. Mater.* **4** 816–9